Preprint, published in Combustion and Flame 210 (2019) 467-478.
https://doi.org/10.1016/j.combustflame.2019.09.002

Hot surface ignition dynamics in premixed hydrogen-air near the lean flammability limit

L.R. Boeck*[a], J. Melguizo-Gavilanes[a,b], J.E. Shepherd[a]

[a]*Graduate Aerospace Laboratories, California Institute of Technology, Pasadena, CA 91125, USA*
[b]*Institut Pprime, UPR 3346 CNRS, ISAE–ENSMA, BP 40109, 86961 Futuroscope–Chasseneuil Cedex, France*

Abstract

The dynamics of ignition of premixed hydrogen-air from a hot glow plug were investigated in a combined experimental and numerical study. Surface temperatures during heating and at ignition were obtained from 2-color pyrometry, gas temperatures were measured by high-speed Mach-Zehnder interferometry, and far-field effects were captured by high-speed schlieren imaging. Numerical simulations considered detailed chemical kinetics and differential diffusion effects. In addition to the known cyclic (puffing) combustion phenomenon, singular ignition events (single puff) were observed near the lean flammability limit. Detailed analysis of the results of our numerical simulations reveal the existence of multiple combustion transients within the thermal boundary layer following the initial ignition event and, at late times, sustained chemical reaction within a thermal plume above the glow plug. The results have significant implications for ignition from hot surfaces within near-flammability limit mixtures at the edge of plumes resulting from accidental release of hydrogen or within the containments of nuclear power plants during severe accidents.

Keywords: Experiments; Hot surface; Hydrogen; Ignition; Numerical simulation

1. Introduction

Combustion of premixed hydrogen-air atmospheres near the lean flammability limit exhibits a rich variety of behavior. The very low (less than 10 cm/s for hydrogen concentrations less than 10% [1, 2]) burning speeds, high diffusivity of hydrogen and the negative Markstein lengths result in a strong coupling of chemistry and hydrodynamics in lean mixtures. This coupling [3] results in significant effect of flame stretch as well as the potential for thermal-diffusive and Landau-Darrieus instabilities, resulting in local extinction

and significant geometric distortion of the flame surface even in otherwise laminar flows [1].

The combustion chemistry of hydrogen-air mixtures has been examined by many researchers, Sanchez and Williams [4] provide an extensive review with sections 6.3 and 6.6 specifically addressing lean combustion issues, which involve the competition between OH and HO_2 and H_2O_2 reactions. In mixtures near the flammability limits, it has long been known [5, 6], that buoyancy strongly affects the flame propagation. The effect of buoyancy is pronounced in lean hydrogen-air mixtures and the interaction of propagating flames with gravity in normal and micro-gravity conditions has been examined by a number of researchers [7–10]. Near-limit mixtures exhibit a number of unusual combustion phenomena such as flame balls [11].

The topic of ignition by hot surfaces has been examined extensively from the beginnings of combustion science in the 19th century and continuing today as the subject of both fundamental and applied research. Analytical studies of ignition within the boundary layer of hot surfaces have focused on the balance between energy release, heat transfer and reactant depletion within the gas [12–17] as well as the role of conjugate heat transfer between gas and surface [18] and the role of thermal diffusion [19] by hydrogen. Recent studies on thermal ignition by hot particles [20–22] in hydrogen-oxygen-diluent mixtures have focused on examining the ability to both measure and predict through either numerical simulation or correlation the dependence of ignition thresholds on particle material, size and heating rate.

Applied research studies have focused on measuring [23, 24] and predicting the minimum surface temperature required to ignite a flammable mixture (i.e., the ignition threshold). This metric is a function of the mixture composition, hot surface size, orientation, shape and material, as well as the relative velocity between gas and hot surface [25]. Many of these studies have been motivated by nuclear reactor safety and were carried out in the 1980s [26] in which hot surfaces (glow plugs) were used to ignite hydrogen at lean conditions. Loss-of-coolant accidents in nuclear reactors can potentially result in the release of significant quantities of hydrogen and the generation of flammable atmospheres within the containment, which occurred at Three Mile Island Unit 2 in 1979 [27] and in Units 1, 3 and 4 at Fukushima Dai-ichi in 2011 [28]. One strategy initially considered for mitigating explosive overpressure was to perform deliberate ignition by glow plugs located inside nuclear reactor containments. The emphasis in the last two decades has shifted to passive autocatalytic recombiners for ultra-lean hydrogen combustion in nuclear power plants with contributions from engineering studies [29, 30], analysis [31], numerical simulation [32], and surface science [33].

Another motivation for studying near-limit combustion and ignition processes is the proposed use of hydrogen as an energy carrier, and the continuing use of hydrogen in chemical processes and as a coolant in large-scale electric power generation. Accidental releases and explosions pose an inherent potential hazard, and ignition of flammable clouds created by accidental release of hydrogen from production, transportation or storage facilities is of continued interest.

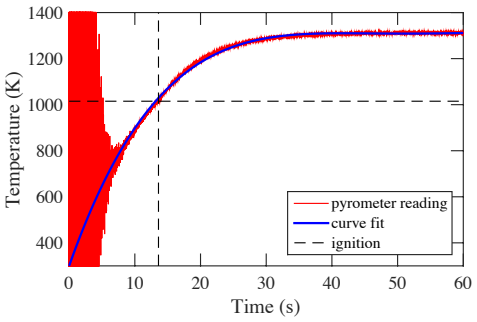

Figure 1: Glow plug surface temperature evolution during heating, measured by 2-color pyrometry.

In the presence of continuous thermal ignition sources, Boettcher et al. [34], observed cyclic (puffing) flame propagation in near-limit premixed mixtures using hydrocarbon fuels. This regime is characterized by the repeated formation of a flame near the hot surface followed by propagation upward within the thermal plume above the thermal igniter. The present work is motivated by these observations and examines in-depth the regime of lean, near-limit hydrogen-air mixtures (X_{H_2} = 5-6%, ϕ = 0.125-0.15), the limiting case of the puffing behavior in which only a single puff is observed. This phenomenon was first noticed by Boettcher [35] (see p. 127) and we refer to this as the "single-puff regime". The objective of the present work is the characterization of single-puff behavior using a combined experimental and numerical approach.

2. Experimental methodology

2.1. Combustion vessel and procedure

Ignition experiments were conducted in a prismatic vessel whose internal dimensions were 0.114 m (W) x 0.114 m (D) x 0.165 m (H). The hot surface, a cylindrical Autolite 1110 glow plug with a stainless steel 316 surface, was mounted vertically in the lower section of the vessel and equipped with a horizontal stagnation plate at the bottom, used to provide a defined flow boundary condition. The glow plug diameter was 5.1 mm, and the height above the stagnation plate exposed to the mixture was 9.3 mm. This setup has been used in previous work and is described in detail in [34].

The experiment was performed as follows: the vessel was evacuated and filled with hydrogen, oxygen and nitrogen ($X_{O_2} : X_{N_2}$ = 1 : 3.76) using the method of partial pressures with a 10 Pa measurement accuracy. The components were mixed by a circulation pump and left to settle for 180 s. The initial conditions before the start of glow plug heating were P_o = 101.3 $\pm$ 0.1 kPa and T_o = 296 $\pm$ 3 K. Supplying electrical current to the glow plug initiated the heating. The glow plug current and voltage were chosen such that fast initial heating was achieved and temperature was stabilized subsequently, see Fig. 1. Each experiment was terminated after 60 s.

2.2. Diagnostics

Ignition was characterized in terms of glow plug surface temperature, measured by 2-color pyrometry, gas temperature fields in the vicinity of the glow plug, measured by high-speed Mach-Zehnder interferometry, and the far-field was captured by high-speed schlieren imaging.

2.2.1. Surface temperature measurement by 2-color pyrometry

A two-color pyrometer was used to measure the glow plug surface temperature as a function of time. The construction and calibration of the pyrometer, using a black-body source, is described in [36]. Pyrometry allows for non-contact temperature measurement, not affecting the boundary layer near the hot surface; measurement errors pertaining to thermocouple measurements of hot surface temperatures, related to radiative, convective and conductive losses from the junction, thermal contact resistance, and surface reactions, are eliminated. The pyrometry measurements were additionally validated using interferometry [36]. The pyrometer field-of-view had a Gaussian sensitivity profile with a FWHM of 1.0 mm. Optical access to the glow plug was restricted such that the pyrometer could only measure the temperature of the side wall near the glow plug top, $z \approx 8.5$ mm. Since ignition consistently took place on the symmetry axis above the glow plug top face, by translating the pyrometer we determined that the top face temperature was about 2.5% lower than the temperature at the pyrometer measurement location. This deviation was included in the ignition threshold measurement uncertainty along with emissivity corrections, measurement noise and calibration uncertainty. The total estimated measurement uncertainty is represented by error bars on the plots.

Ignition events were identified using high-speed interferograms, which clearly show the incipient ignition kernel, compared to no-ignition cases (see, for example, ignition kernel above the glow plug in Fig. 3, $t = t_{\text{ref}}$). The ignition threshold was determined by reading the surface temperature of the glow plug, measured by 2-color pyrometry, at the time the ignition kernel first became visible in the interferograms.

2.2.2. Gas temperature measurement by high-speed Mach-Zehnder interferometry

The gas temperature in the vicinity of the glow plug was inferred from interferograms obtained from a Mach-Zehnder interferometer and high-speed video camera, operating at a framing rate of 2000 fps and a resolution of 800×800 px^2, covering a field-of-view of about 25×25 mm^2. The interferometer measured variations in refractive index inside the combustion vessel. Temperature variations were computed from interferograms using the methodology described in [36, 37].

2.2.3. Far-field characterization by high-speed schlieren imaging

A classical Z-type schlieren setup was used to qualitatively image the gas-density gradients associated with thermal plume and flame, in the entire optically accessible region of the vessel. This extends the

smaller region observed by the Mach-Zehnder interferometer and enables direct comparison with numerical simulations, which cover the entire vessel domain.

3. Computational methodology

The motion, transport and chemical reaction in the gas surrounding the glow plug were modeled using the low Mach number, variable-density reactive Navier-Stokes equations with temperature-dependent transport properties [38]. Differential diffusion effects were taken into account using a constant but non-unity Lewis number for each species [38]. The Lewis numbers were computed for the specific investigated conditions. A detailed description and validation of the model can be found in [39]. The governing equations were solved in an axisymmetric 2-D geometry (a 5 degree wedge with its axis of rotational symmetry located along the z-axis at $x = 0$) using the OpenFOAM toolbox [40]. The chemistry was modeled using Mével's mechanism for hydrogen oxidation, which includes 9 species and 21 reactions [41, 42]. A detailed comparison of the ignition delay time performance of Mével's mechanism with others commonly used in the literature is provided in [43, 44]. The main challenge in simulating very lean mixtures lies in the fact that the concentrations of interest ($X_{\mathrm{H_2}}$ = 5%) fall outside the range in which these mechanisms are typically validated ($9.5\% \leq X_{\mathrm{H_2}} \leq 63\%$). However, as will be shown below, this kinetic mechanism does a very good job at reproducing the experimentally observed dynamics before, during and after ignition without requiring any modification.

The computational domain was discretized with 200,000 cells, compressed near the wall of the glow plug with a minimum cell size of 80 μm, to resolve the thermal and hydrodynamic boundary layers. A resolution study resulted in the grid size chosen. Additionally, a thorough validation of the ability of our numerical model to predict the heat transfer was performed in [37, 39] via a side-to-side comparison of experimental and numerical temperature fields and profiles around the hot surface and thermal plume. The initial conditions were P_o = 101 kPa, T_o = 300 K, U_o = (0,0) m/s, and mass fractions $Y_{\mathrm{H_2}}$ = 0.00364, $Y_{\mathrm{O_2}}$ = 0.23216, $Y_{\mathrm{N_2}}$ = 0.7642, corresponding to a hydrogen mole fraction of $X_{\mathrm{H_2}}$ = 5%. A no-slip boundary condition and constant temperature, $T_{\mathrm{wall}} = T_o$, were imposed on the vessel walls. On the glow plug surface, the experimental temperature-time history measured by pyrometry as shown in Fig. 1 was imposed uniformly on the entire glow plug surface. The simulation was carried out as an initial value problem, integrating in time starting from quiescent initial conditions with ignition and flame propagation being computed as part of the solution, rather than artificially igniting the mixture or imposing a prescribed flame speed as was done in [34]. The numerical ignition criterion was defined as $T_{\mathrm{ign}} = T_{\mathrm{surf}} + 150$ K.

4. Results

Section 4.1 provides ignition thresholds and temperature fields measured experimentally, and Sec. 4.2 shows numerical results in comparison with experimental results, analyzing the ignition process in detail.

4.1. Experimental ignition thresholds and temperature fields

Figure 2 presents ignition thresholds as a function of hydrogen mole fraction between the flammability limits. Ignition thresholds increase with increasing hydrogen mole fraction, from 1010 K at X_{H_2} = 5% to 1100 K at X_{H_2} = 70%, and an additional steep increase occurs near the upper flammability limit, up to 1170 K at X_{H_2} = 73%. As previous research summarized in [43] has shown, ignition thresholds of hydrogen-air mixtures for small hot surfaces with dimensions on the order of 1-10 mm range above 1000 K and increase with increasing hydrogen concentration. As shown by Kutcha et al. [23], ignition thresholds increase with decreasing hot surface size, due to increased heat losses and reduced residence time of gas near the hot surface. As the temperatures increase above 900-1000 K, chain-branching reactions become increasingly more relevant as compared to reactions forming peroxides [39, 43]. This leads to a sharp decrease in ignition delay time with increasing surface temperature and enables ignition to occur when ignition delay time and gas residence time near the hot surface become comparable. Numerical simulations indicate that the increase in ignition threshold with increasing hydrogen concentration may be related to the removal of H and HO_2 through surface reactions [43].

Between the flammability limits, we observed the following ignition regimes: (i) at $X_{H_2} \geq 10\%$, expanding flames occurred with a steady consumption of the entire vessel volume; (ii) at X_{H_2} = 9%, a buoyant flame occurred that propagated towards the vessel top and recirculated along the vessel side walls towards the vessel bottom; (iii) at $7\% \leq X_{H_2} \leq 8\%$ cyclic (puffing) combustion took place. In this regime ignition takes place periodically at the hot surface. Boettcher et al. [34] described the fluid mechanics of this regime in detail for *n*-hexane-air mixtures; (iv) at $5\% \leq X_{H_2} \leq 6\%$, we observed single-puff ignition events, which had previously been observed, but not examined in detail by Boettcher [35]. We define a single-puff as a single ignition event, in contrast to the periodic ignition of fresh mixture near the hot surface in the case of cyclic (puffing) flames. The single-puff first manifests itself as an ignition kernel near the hot surface and subsequently produces a region of high temperature attached to the hot surface. In contrast to expanding flames, this high-temperature region does not expand laterally into the fresh mixture, but is confined to a narrow vertical region bounded by the thermal plume above the hot surface. No further ignition kernels appear near the hot surface within the observed time frame of 60 s. The detailed mechanism of single-puff ignition is described next.

Gas temperature fields inferred from Mach-Zehnder interferometry are presented in Fig. 3 for X_{H_2} = 5%. The first frame, $t = t_{ref} - 12.5$ ms, corresponds to a glow plug surface temperature of 1010 K, where

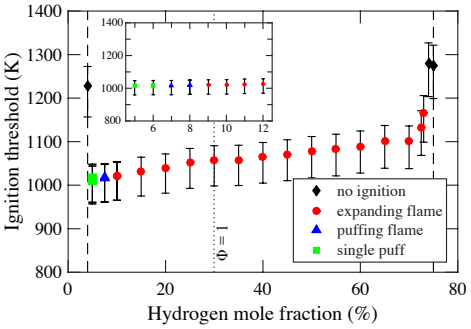

Figure 2: Ignition thresholds and ignition regimes (markers) as a function of hydrogen mole fraction.

$t = t_{\text{ref}}$ refers to the first appearance of an ignition kernel in the experiment. The leading edge of the flame subsequently propagates upwards within the thermal plume, while the bottom part of the flame propagates downwards along the glow plug sides, reaching a minimum height of about $z \approx 4$ mm, at $t = t_{\text{ref}} + 12.5$ ms. At $t = t_{\text{ref}} + 25$ ms, a characteristic concave flame section can be seen at $z \approx 10$ mm and $x \approx 4$ mm. This section travels upwards subsequently. At later times, $t > t_{\text{ref}} + 1$ s, a plume of hot gas is visible in the temperature fields above the glow plug. The gas in this region is at distinctly higher temperature than the gas within the initial thermal plume above the glow plug, at $t = t_{\text{ref}} - 12.5$ ms. Numerical simulations will help evaluate this situation in more detail.

4.2. Numerical results and comparisons against experiments

Figure 4 shows a comparison of experimental and numerical schlieren sequences for a single-puff event in a 5% hydrogen-air mixture. Numerical schlieren images display the gradient of the density field; the optical details of the experimental schlieren imaging process were not computed. As a result, differences in intensity between the experimental and numerical images are expected, particularly on the centerline of the fields. The widths of the thermal plume and boundary layer, above and near the surface of the glow plug, respectively, are predicted with reasonable accuracy for all the time instances shown. At $t = t_{\text{ref}}$, there are only slight discrepancies regarding the location of the tip of the flame during the main ignition transient; for $t > t_{\text{ref}}$, the flame shape during its propagation along the plume is captured by the simulation. Additional experimental schlieren sequences are included in the supplemental material, providing an overview of the different ignition regimes referred to in Fig. 2, and demonstrating that single-puff ignition can also be obtained from smaller ignition sources heated at higher rates, such as a heated wire, and is therefore not specific to the geometry at hand.

For $X_{\text{H}_2} = 5\%$, the simulation predicts an ignition threshold of 938 K, 7.1% lower than the value we observe experimentally (1010 K). Due to this difference in ignition temperature, it is not informative to present experimental and numerical temperature fields side-by-side. In [39] a thorough investigation of the ignition dynamics was performed in which we studied the physical and chemical mechanisms that play a

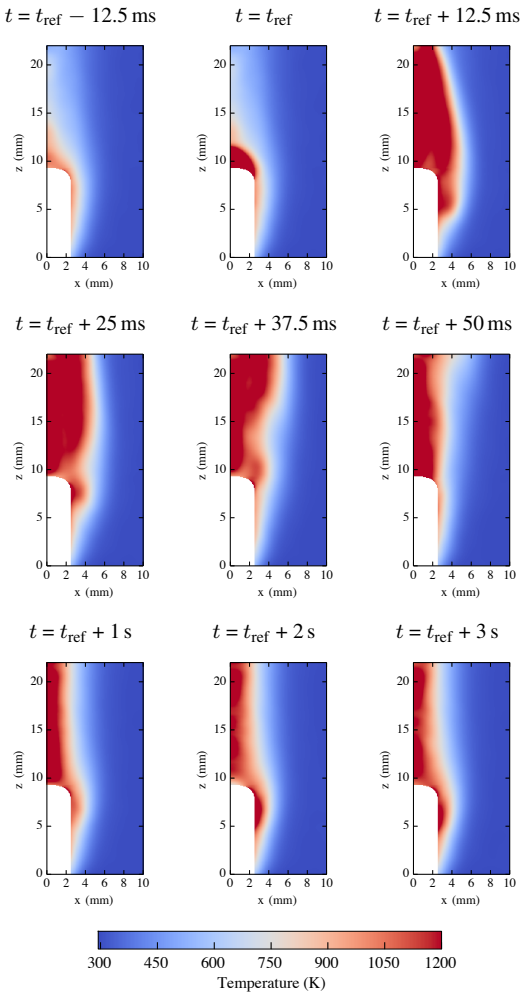

Figure 3: Single-puff ignition in 5% hydrogen-air mixture. Temperature fields inferred from experimental finite-fringe interferograms.

role in thermal ignition, including chemical pathways. Additionally, in [43], we discussed various effects that could affect the experimentally reported and numerically predicted thresholds, such as non-uniform heating of the hot surface and surface reactions in the experiments, and the choice of reaction mechanism in the simulation. Different reaction mechanisms compared in [43] showed large discrepancies in terms of ignition delay time predictions near the present ignition thresholds ($\sim 900-1000$ K). Rows 1 and 2 in Fig. 5 show numerical temperature and velocity (magnitude) fields, along with velocity vectors revealing the flow dynamics inside the combustion vessel. Row 3 presents corresponding OH and HO_2 mass fractions. Ignition occurs at the glow plug top evidenced by an increase in temperature and OH and HO_2 mass fractions. At $t = t_{ref}$, a flame can be seen, propagating upward within the thermal plume. The maximum in velocity remains inside the plume indicating weak expansion of the gas during the ignition/flame propagation event. However, it does induce an appreciable horizontal velocity that disturbs the streamlines as shown at $t = t_{ref}$ compared to $t = t_{ref} - 12.5$ ms. The flame remains anchored at the outer top edge of the glow plug throughout the majority of the process. The temperature and velocity fields, and streamlines show the

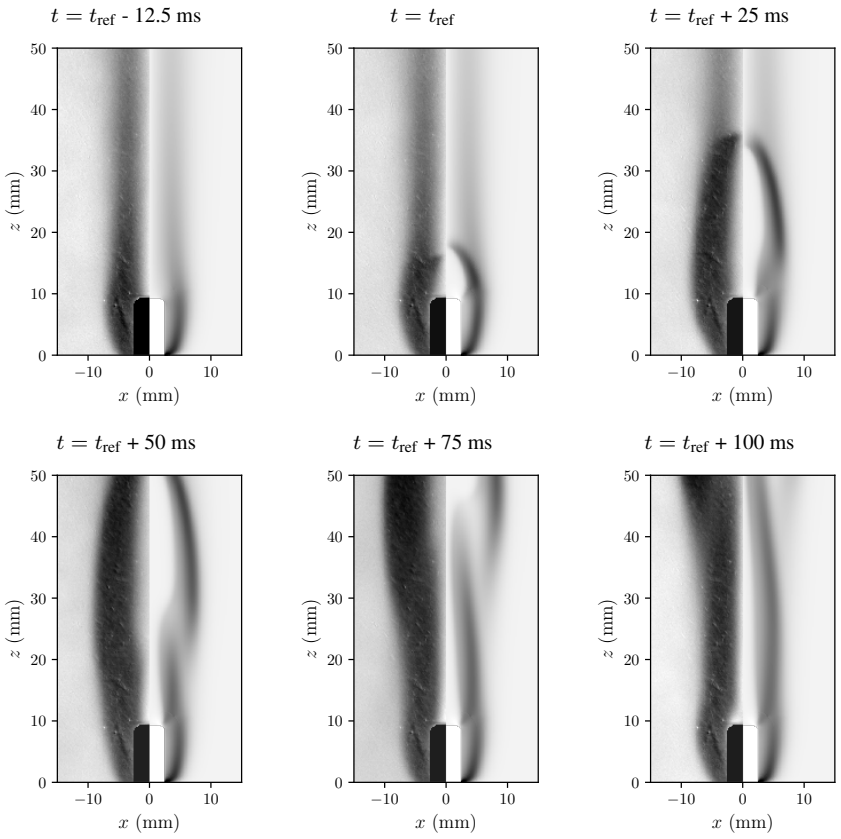

Figure 4: Side-by-side comparison of schlieren fields for a single-puff event in a 5% hydrogen-air mixture. Left: experimental; right: numerical.

formation of a vortical structure at the edge of the flame, see for instance at $t = t_{\text{ref}} + 25$ ms at $z \approx 20$ mm and $x \approx -10$ mm, which leads to a localized concave deformation of the flame as observed in the experiments. This is the result of the horizontal velocity induced by the ignition event and the vertical buoyancy flow induced by the heating of the glow plug. This vortex gets advected upwards, and results in complete detachment of the top portion of the flame at later times (not shown). The early stages of the vortex-flame interaction can be observed at $t_{\text{ref}} + 25\,\text{ms} \leq t \leq t_{\text{ref}} + 50\,\text{ms}$ around $z = 25$ mm in Fig. 5. The evolution just described is consistent with the experimental observations in Fig. 3; the experiment shows additional side ignitions at $t = t_{\text{ref}} + 12.5$ ms and $t_{\text{ref}} + 25$ ms. While side ignitions do take place numerically (see Fig. 7) they do not seem to be as strong or to occur at the same time as in the experimental fields shown in Fig. 3. This discrepancy is very likely due to the non-uniformity in surface temperature in the experimental glow plug alluded to earlier. In the surface temperature range at hand (~ 1000 K), the experimental temperature non-uniformity of 2.5 % quoted above (~ 25 K) induces an appreciable change in ignition delay time that make side ignitions more likely to occur experimentally than numerically [43].

Figure 6 shows OH and HO_2 mass fractions (row 1), and H mass fraction and hydrogen concentration (row 2), at late times after the initial ignition transient, 1 s, 2 s and 3 s after ignition. A vertical plume of

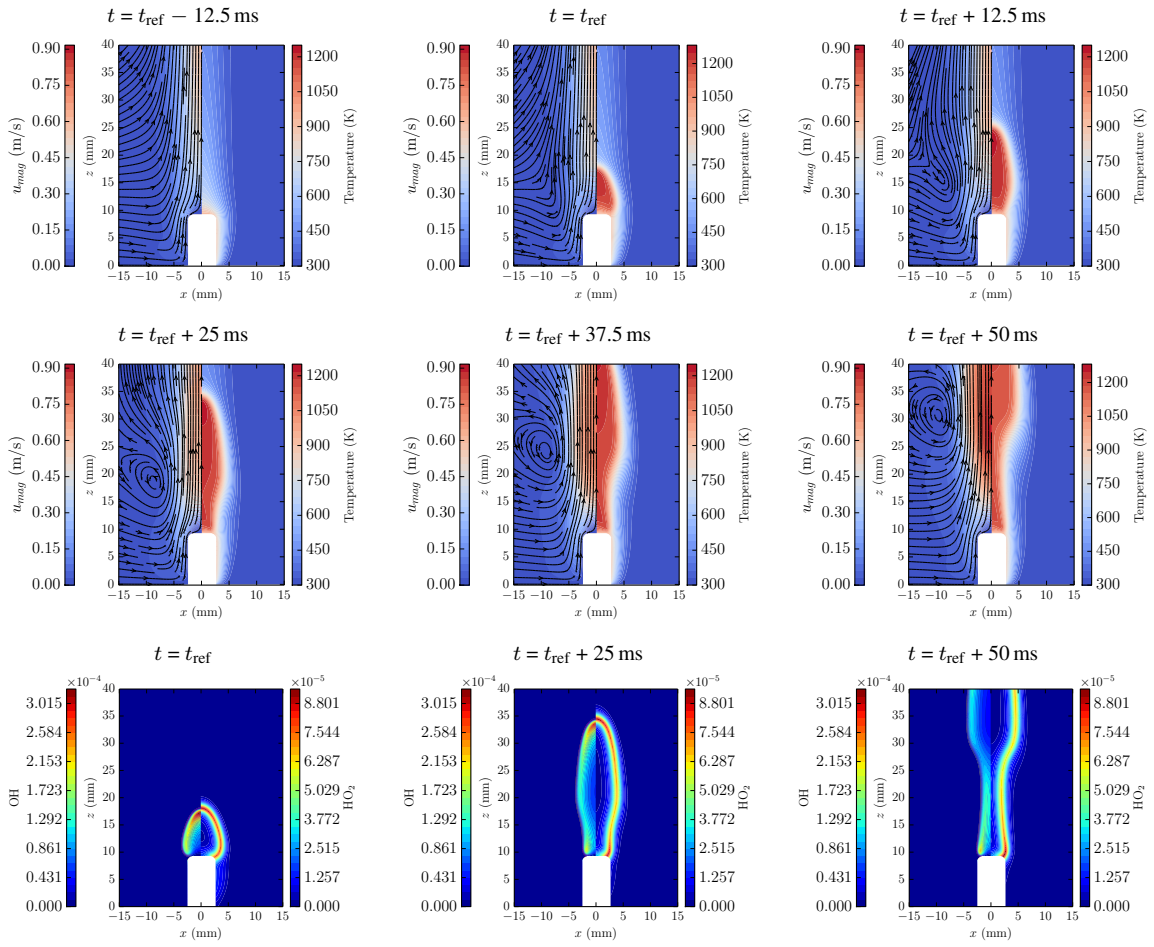

Figure 5: Temperature and velocity (magnitude) fields, streamlines and mass fraction (OH, HO_2) fields during ignition and flame propagation for a 5% hydrogen-air mixture; early times.

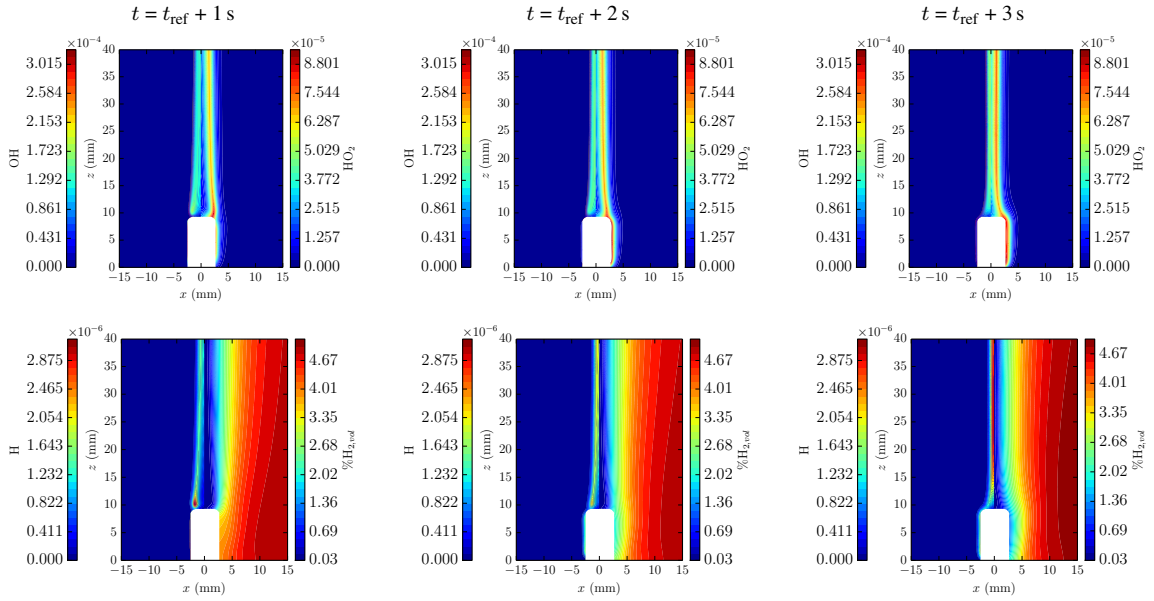

Figure 6: Mass fractions (OH, HO_2, H) and hydrogen concentration fields after ignition for a 5% hydrogen-air mixture; late times.

combustion products is observed, fed by reactants from the sides of the glow plug. Production of OH decays from $t = t_{\text{ref}} + 50\,\text{ms}$ to $t = t_{\text{ref}} + 1\,\text{s}$, whereas HO_2 continues to be strong at the top edge and side of the hot surface. One second after ignition, the sides of the glow plug are surrounded by mixture that is slightly below the lower flammability limit of hydrogen-air (4%). See Fig. 6, row 2. At $t = t_{\text{ref}} + 2\,\text{s}$ and $t = t_{\text{ref}} + 3\,\text{s}$, the fields show a further decrease in H_2 content with values ranging from 1–3% within the thermal boundary layer. There is partial conversion of H_2 to HO_2 but not enough H atoms are present to result in the production of OH through reaction $H + HO_2 \rightarrow OH + OH$. In contrast, the production of OH and H is significant in the thermal plume although weak at the top edges on the glow plug. In agreement with the experiment, no further large ignition events are observed in the simulation.

5. Discussion

The dynamics of ignition from a hot surface in premixed hydrogen-air at the lean flammability limit differ from mixtures at higher hydrogen concentrations. The strong effect of buoyancy and the low energy content of the mixture lead to dynamics that include a primary ignition event, decay of the initial ignition transient, and, at late times, establishment of a quasi-steady flow field that features a region of high temperature with sustained chemical reaction, which extends vertically away from the hot surface. The behavior at late times is most noteworthy, given that premixed flammable mixture surrounds the hot surface, but no flame propagation is observed into the mixture so that chemical reaction, heat release and high temperatures remain confined to the narrow thermal plume above the hot surface. The following analyses further explore the late phenomena after the decay of the initial ignition transient, for $X_{H_2} = 5\%$.

At late times ($t_{\text{ref}} + 1\,\text{s} \leq t \leq t_{\text{ref}} + 3\,\text{s}$), the glow plug surface is surrounded by a layer of gas that is depleted in hydrogen below the flammability limit. The thermal plume above the glow plug induces motion in the bulk gas entraining fresh reactants into the thermal boundary layer surrounding the glow plug. Ignition will not occur within the boundary layer as long as the convective time scale τ_{conv} (approximately the ratio of the height of the glow plug to the velocity induced by buoyancy) is shorter than the chemical time scale τ_{chem} (i.e. ignition delay time of the mixture). If τ_{chem} is shorter than τ_{conv}, ignition is possible on the side of the glow plug. The relative magnitude of these time scales changes significantly as the surface temperature of the glow plug continues to increase after ignition due to heating, see Fig. 1. Due to the strong dependence of the chain-branching chemical reaction rates on temperature, a small increase in surface temperature results in a significant decrease in τ_{chem}. While $\tau_{\text{conv}}/\tau_{\text{chem}} \leq 1$, fresh mixture travels along the side of the glow plug and burns at the top edges feeding the thermal plume with hot products. As soon as $\tau_{\text{conv}}/\tau_{\text{chem}} > 1$ ignition can occur at the side of the glow plug and its top edges are now fed by combustion products or partially reacted mixture. This explains the decrease observed in OH and H_2 concentration within and above the thermal boundary layer for $t_{\text{ref}} + 50\,\text{ms} \leq t \leq t_{\text{ref}} + 3\,\text{s}$.

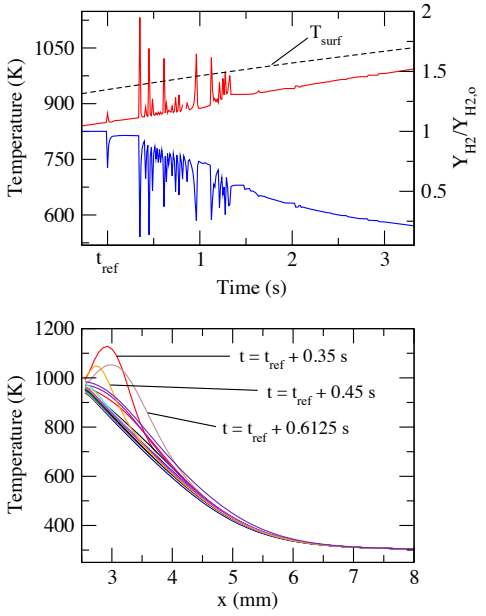

Figure 7: Side ignition events, X_{H_2} = 5% - Top: numerical probes of temperature and normalized fuel mass fraction ($Y_{H2}/Y_{H2,o}$) taken at z = 5 mm and 0.35 mm away from the side surface of the glow plug. Probes taken every 12.5 ms (f = 80 Hz). Bottom: numerical temperature distributions within thermal boundary layer at z = 5 mm for t_{ref} + 0.325 s $\leq t \leq t_{ref}$ + 2 s.

In Fig. 7 (top), we plot temperature (red) and normalized fuel mass fraction (blue) on the side of the glow plug at z = 5 mm and a distance of 0.35 mm away from the wall. The first transient observed at t_{ref} is the signature of the primary ignition event. For 0.3 s after the primary ignition event, the gas temperature remains about 100 K less than the imposed temperature on the glow plug surface (black dashed line), due to the steep temperature gradient within the thermal boundary layer at the glow plug wall. At $t = t_{ref}$ + 0.35 s, a second transient in temperature and a corresponding decrease in fuel mass fraction are observed. Subsequently, a series of transient combustion events occur as the fuel is entrained into the boundary layer, ignites, depleting the fuel and repeating the cycle as fresh mixture is entrained. This continues until approximately $t = t_{ref}$ + 1.3 s. As discussed in subsection 4.1, experimental side ignitions were also observed during the main ignition event (see Fig. 3). However, experimentally capturing the weak temperature peaks at the frequency reported in our simulations at late times is beyond our current experimental capabilities.

Fig. 7 (bottom) shows the radial distribution of temperature within the thermal boundary layer at z = 5 mm. The ignition events are accompanied by the peaks in temperature that occur within 1 mm of the surface. None of these combustion transients result in a self-sustained flame and the temperature increase remains confined to the thermal boundary layer. We speculate that we do not observe further combustion transients after $t \sim t_{ref}$ + 1.5 s because as the temperature of the glow plug continues to increase, $\tau_{conv}/\tau_{chem} \gg 1$, which results in transients occurring at a higher frequency than we are sampling the simulation output (f = 80 Hz).

To examine the processes in the plume above the glow plug, we have investigated the temperature

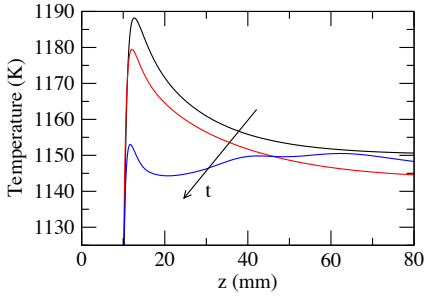

Figure 8: Numerical temperature distribution along thermal plume at $x = 0$ mm for t_{ref} + 1 s (black), t_{ref} + 2 s (red) and t_{ref} + 3 s (blue); X_{H_2} = 5%.

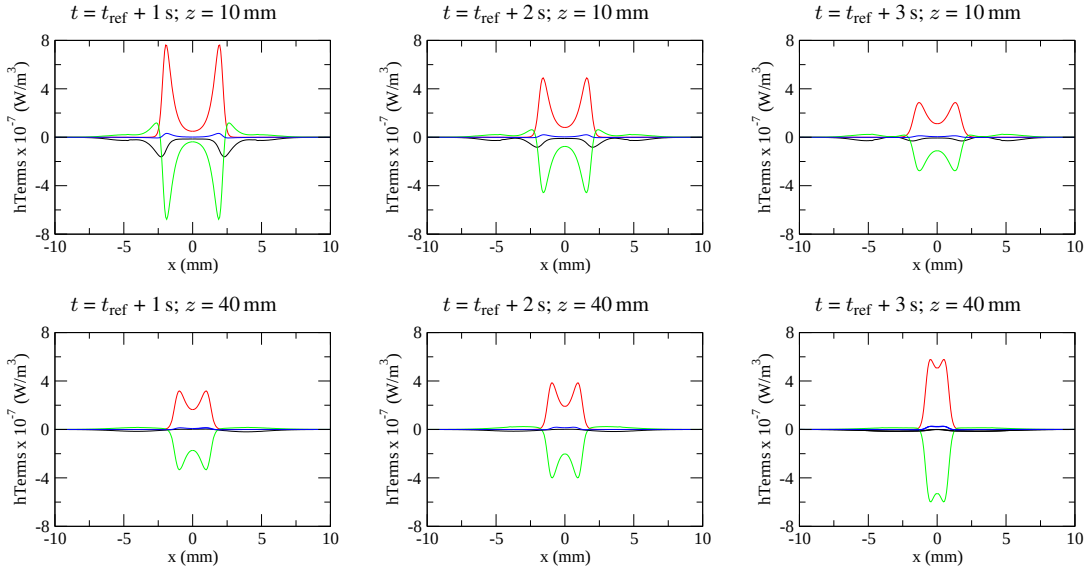

Figure 9: Contributions of each term in the energy equation at two heights, 10 mm and 40 mm, and three times, t_{ref} + 1 s, t_{ref} + 2 s and t_{ref} + 3 s. Convection (black); conduction (green); enthalpy transport due to species diffusion (blue); chemical source term (red); X_{H_2} = 5%.

distributions along the thermal plume as well as the contributions of each term in the energy equation. The temperature distributions along the plume centerline are shown in Fig. 8 for $t = t_{\text{ref}}$ + 1 s, t_{ref} + 2 s and t_{ref} + 3 s. The corresponding surface temperatures at these times are 975 K, 1001 K and 1042 K, respectively, significantly lower than the maximum peak temperature in the figure suggesting that chemical reactions are taking place at this late time.

To investigate this further we plot in Fig. 9 as black, green, blue and red lines respectively, the competition among the different terms in the energy equation: convection, $-\nabla\cdot(\rho\mathbf{u}h_s)$, conduction, $\nabla\cdot(\kappa/c_p\nabla h_s)$, enthalpy transport due to species diffusion, $-\sum_{i=1}^{N-1} h_{s,i}(1-1/\text{Le}_i)\kappa/c_p\nabla Y_i$, and the chemical source term, $-\sum_{i=1}^{N-1}\Delta h^o_{f,i}\dot{\omega}_i$ at two heights, z = 10 mm (top) and z = 40 mm (bottom) for three times,

$t = t_{\text{ref}}$ + 1 s (left), $t = t_{\text{ref}}$ + 2 s (center) and $t = t_{\text{ref}}$ + 3 s (right). A key observation is that for these times and locations, the energy balance appears to be quasi-steady with a dominant balance between conduction of thermal energy and chemical energy release. At z = 10 mm, the main chemical activity and balancing

conduction process occurs directly above the edge of the glow plug ($x \approx \pm$ 2 mm). Outside of this region, chemical reaction is minimal and convection balances conduction. Energy transport due to species diffusion, which accounts for the contribution of differential diffusion effects to the energy balance in the current computation, seems to play a negligible role at these times in all the cases shown in Fig. 9. This term would vanish had we assumed a unity Lewis number formulation. However, including differential diffusion effects is essential to correctly predicting the transport of H_2 and H species, as the differential diffusion of those species is crucial to all aspects of lean hydrogen combustion. This comprises the prediction of flame-balls, tubular flames and conventional laminar flame properties, including: (i) laminar burning velocities, s_L (neglecting it in lean hydrogen-air mixtures results in overpredictions in s_L of a factor of two); (ii) stability (lean hydrogen-air flames are thermodiffusively unstable); and (iii) response of flames to stretch (curvature and strain) [45, 46]. These experimental studies of lean hydrogen-air flames show that even modest stretch rates can increase the burning rate substantially, which may be significant to initiating and sustaining combustion in the very lean mixtures (5% H_2 corresponds to an equivalence ratio of 0.125) used in the present study.

With increasing time, the chemical activity at z = 10 mm decreases as seen in the decreasing magnitude of both the source and balancing conduction terms. Chemical reaction close to the centerline is minimal due to the depletion of hydrogen in this region by the primary ignition event. At z = 40 mm, the chemical activity is most intense in the column of gas near the centerline, increasing in magnitude and becoming smaller in radial extent with increasing time. Radial diffusion and convection by buoyancy induced flow transports hydrogen and air into this region. Numerical evidence suggests that, after the main ignition event, the plume of hot products is initially sustained by burning from the top edges of the glow plug, and at later times the plume is sustained by diffusive burning as the plume starts to shrink and sufficient time for radial diffusion of fuel/partially reacted species is allowed.

To gain additional insight into the structure and nature of the reacting front in the plume at late times we plot in Fig. 10 temperature, species and radial velocity distributions, at the same heights and times as in Fig. 9. The plume consists of an isothermal core surrounded by a reaction zone with two length scales, an inner region defined by a sharp increase in the radical species H, O and OH and chemical energy release and an outer region defined by broad diffusion zones for major products, HO_2, H_2O_2 and temperature with relatively little energy release. A few additional features stand out: (i) the quasi-stationary character of the plume at a fixed height is evident, as well as the high diffusivity of H_2 showing a continuously decreasing profile as it approaches the edge of the plume, whereas O_2 stays mostly flat before chemical reactions take place. See major species and temperature profiles. (ii) the minor species profiles at $z = 10$ mm show a decay in chemical activity and thinning of the plume. In contrast, at $z = 40$ mm, chemical activity increases towards the center of the plume as evidenced by the increasing mass fractions of H and OH with

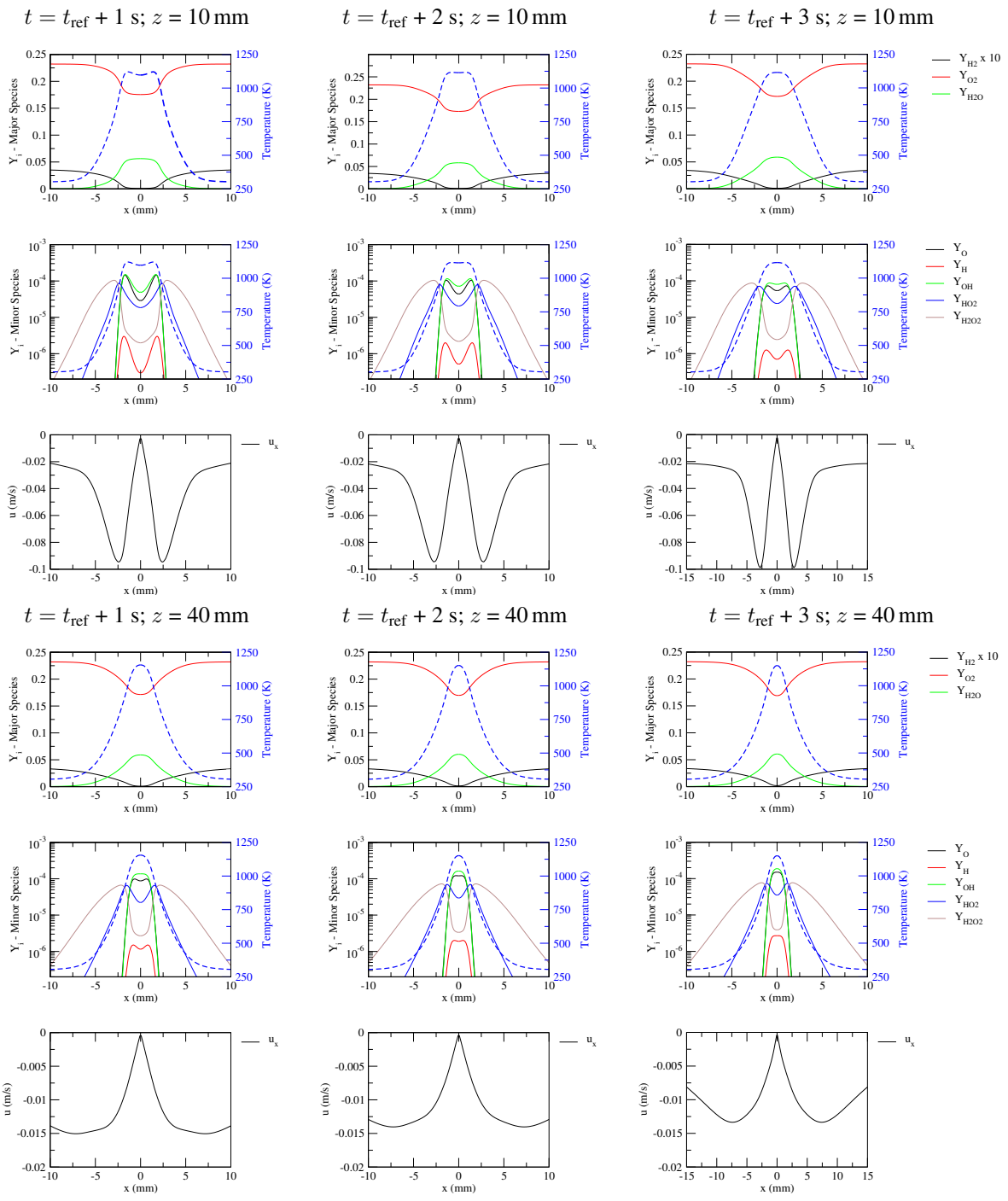

Figure 10: Nature of reacting front at two heights, 10 mm and 40 mm, and three times, t_{ref} + 1 s, t_{ref} + 2 s and t_{ref} + 3 s - Major species, minor species, temperature and velocity distributions; X_{H_2} = 5%.

increasing time. Expectedly, the decrease and subsequent increase in chemical activity along the plume, and its thinning, is consistent with the behavior described earlier when the contributions of each term in the energy equation were analyzed. (iii) the radial inflow velocity could be interpreted as being analogous to a laminar burning speed. Over the three times shown, at the location where the peak in chemical source term

occurs, $u \sim 6.6$ cm/s for $z = 10$ mm; for $z = 40$ mm at the same location, $u \sim 0.4$ cm/s. Notably, although there are no measurements or numerical simulations of planar laminar burning speeds for $X_{H_2} < 11\%$, the magnitude of the radial inflow velocities are consistent with the extrapolations of existing data on burning speed. The reactive plume structure does resemble that of tubular flames [47], and has some similarities to flame balls [48] but there are significant differences. The convective flow of gases into the plume's reaction zone is created by the entrainment of the buoyant plume of products rather than by forced flow in the case of tubular flames or essentially zero net convection in the case of a flame ball.

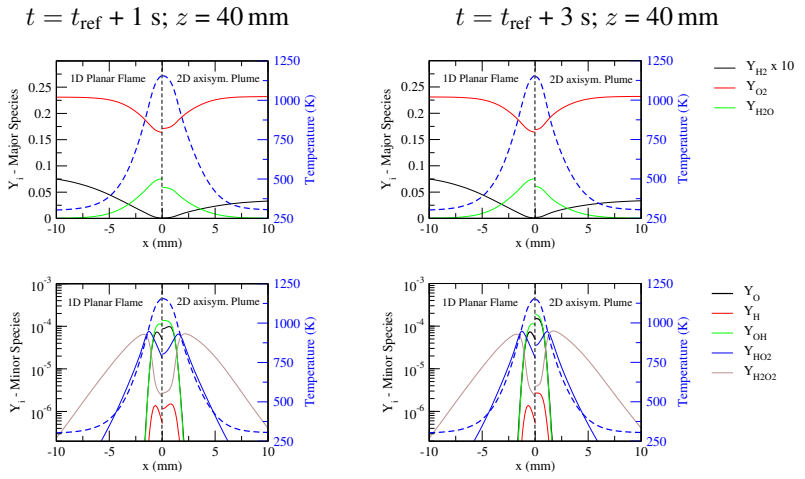

Figure 11: Nature of reacting front at the edge of the plume at one height, 40 mm, and two times, t_{ref} + 1 s and t_{ref} + 3 s; X_{H_2} = 5%. - comparison with 1D planar laminar flame structure at X_{H_2} = 11%.

Figure 11 shows a side-by-side comparison of the reactive structure obtained at the edge of the thermal plume at $z = 40$ mm, and two different times at X_{H_2} = 5%, with that obtained from a 1D planar laminar flame at X_{H_2} = 11%. Discrepancies in the absolute values for some of the quantities shown are to be expected due to differences in geometry (1D vs. 2D-axisymmetric) and hydrogen concentration. In spite of these, the temperature, major and minor species distributions are remarkably similar, which constitutes convincing evidence that the reactive plume at late times is a flame-like structure. The interaction of the flow field with the reaction front and its curved geometry allows for this quasi–steady reacting front to be sustained at conditions where 1D planar flames do not typically exist. In the review paper of Pitz et al. [47] on tubular flames, stretch and curvature effects were discussed at length for fuels with Lewis numbers less and greater than or equal to unity, using burner configurations that deliberately resulted in the behavior naturally observed at late times in our experiments and simulations. Their review emphasized that in this geometry it is possible to have reaction with very lean hydrogen-air mixtures because of the strengthening of flow divergence due to curvature that in turn results in enhanced combustion by differential diffusion. It is therefore plausible that the enhanced combustion/preferential diffusion due to geometry and flow field to which the reacting front is exposed to in our configuration, results in a major/minor species spatial

distribution and flame temperature that happens to be similar to a planar 1D flame at higher hydrogen concentration. Following the definitions in [49, 50], and adjusting them for our case, it can be analytically demonstrated that the total dimensional flame stretch is given by $K = \partial u_z/\partial z$. This result was also derived in [51]. Furthermore, an exact relationship for the flow divergence can also be derived by applying mass conservation across the reacting front: $\partial(\rho u_r)/\partial r = -\rho\left[\partial u_z/\partial z + (u_z/\rho)\partial\rho/\partial z + u_r/r\right]$. Note that the terms on the right hand side represent the effects of flow divergence within the flame (i.e. stretching and curvature); using our simulation results we can determine their values along the plume at the flame location, r_f (i.e. where chemical source term peaks in Fig. 9). The individual contribution of the terms inside the bracket are shown in Fig. 12. Interestingly, the ratio of curvature, u_r/r, to total flame stretch, $\partial u_z/\partial z$, is constant along the plume, with the contribution from stretch being roughly twice that of curvature, providing further evidence of the quasi-steady nature of the reacting front at late times. The remaining term has a very minor contribution to the total flow divergence, with its ratio to stretch reaching values of ~ 0.15 at most (not shown). It seems that this flame-like structure is stationary in the radial direction because the convective motion outward is balanced by the radial inflow due to entrainment by the plume. There is a corresponding increase in the axial mass flow of burned gas in the core of the plume that balances the inflow.

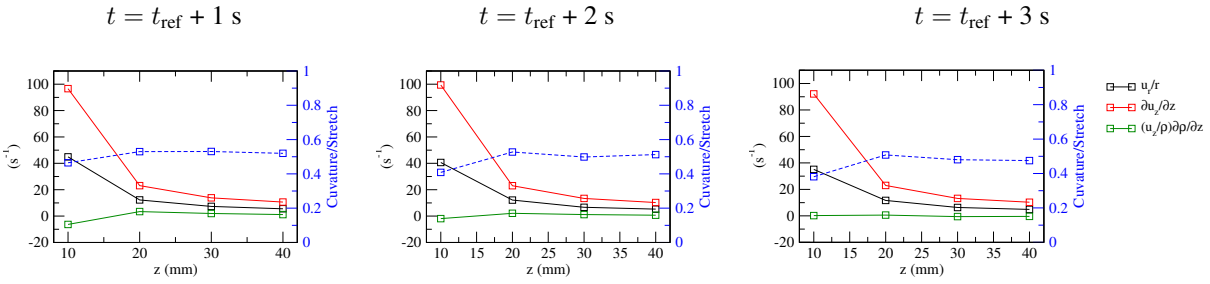

Figure 12: Individual contributions of $\partial u_z/\partial z$, $(u_z/\rho)\partial\rho/\partial z$, and u_r/r to flow divergence, and ratio of curvature to stretch, at the edge of the plume as a function of height, and three times, t_{ref} + 1 s, t_{ref} + 2 s and t_{ref} + 3 s; X_{H_2} = 5%.

Finally, to highlight the effects of differential diffusion due to flow divergence at late stages, the normalized fuel mass fraction is plotted in normalized temperature space for $z = 40$ mm in Fig. 13. The profiles show the typical reacting front structure for fuels with Lewis numbers less than unity [52]. The black line on the plot is a visual aid that approximates the expected behavior of this front for unity Lewis number. Differential diffusion is an essential aspect of the burning at late times.

6. Conclusions

The dynamics of ignition of premixed hydrogen-air from a hot glow plug were studied. In addition to the known cyclic (puffing) combustion phenomenon, we observed single ignition events (single puff) near the lean flammability limit, between hydrogen concentrations of 5 and 6%. The evolution of the single

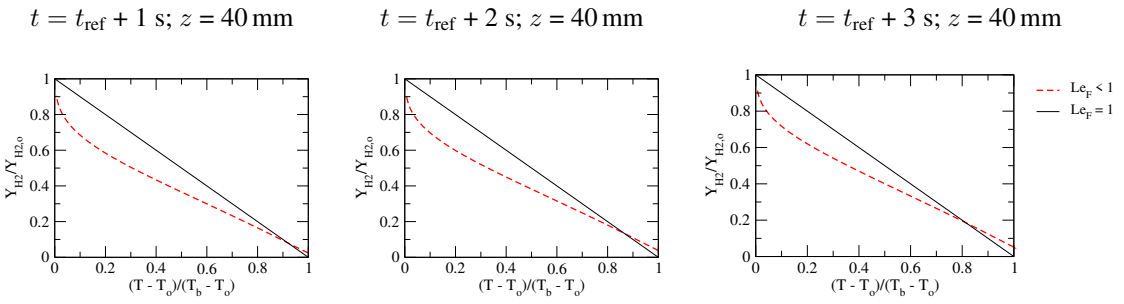

Figure 13: Normalized fuel mass fraction ($Y_{H2}/Y_{H2,o}$) vs. normalized temperature $(T - T_o)/(T_b - T_o)$ at a fixed height $z = 40$ mm, and three times, t_{ref} + 1 s, t_{ref} + 2 s and t_{ref} + 3 s; X_{H_2} = 5%.

puff takes place in four distinct stages: (i) primary ignition event occurring at the top of the glow plug; (ii) constant feed of fresh mixture from the sides of the glow plug to its top edges resulting in an anchored reaction zone and a plume filled with hot products as long as $\tau_{conv}/\tau_{chem} \leq 1$; (iii) repeated combustion transients within the thermal boundary layer at increasing frequency for $\tau_{conv}/\tau_{chem} > 1$ and shielding of the glow plug with mixture depleted in hydrogen below the flammability limit; (iv) chemical reaction in the plume once enough time is available for radial diffusion of fresh reactants into the plume. The flame-like structure is stationary with radial burning velocities on the order of 0.4-6.6 cm/s, balanced by the entrainment of fresh mixture into the plume. The interaction of the flow field with the reacting front at the edge of the plume resulted in a stretched flame that burned at conditions where 1D planar flames do not typically exist. Estimates of the contributions from curvature and stretch to the total flow divergence revealed that the ratio of curvature to stretch was constant along the plume with the contribution from stretch being roughly twice that of curvature. For lean hydrogen-air, positively curved flames strengthen flow divergence and enhance the effects of stretch. Differential diffusion plays an important role in the burning at late times.

When ignition from a hot surface occurs at the boundary of a cloud of hydrogen created by accidental release, the initial ignition transient may not result in a propagating flame but will produce a high-temperature region that extends vertically upward from the hot surface. This applies to the regimes of single-puff ignition and puffing flames, at hydrogen concentrations of 5-6% and 6-8%, respectively. In the single-puff regime, the hot plume of products extending above the hot surface may act as an ignition source for more reactive regions of the cloud, for example it may ignite richer regions of a stratified hydrogen-air layer above the hot surface; the same applies to puffing flames extending from a hot surface into more reactive regions.

Acknowledgements

The present work was carried out in the Explosion Dynamics Laboratory of the California Institute of Technology and was supported by The Boeing Company through a Strategic Research and Development

Relationship Agreement CT-BA-GTA-1. This work used the Extreme Science and Engineering Discovery Environment (XSEDE), which is supported by the National Science Foundation grant number ACI-1548562.

References

[1] D. Bradley, M. Lawes, K. Liu, S. Verhelst, R. Woolley, Laminar burning velocities of lean hydrogen–air mixtures at pressures up to 1.0 MPa, Combust. Flame 149 (1-2) (2007) 162–172.

[2] V. A. Alekseev, M. Christensen, E. Berrocal, E. J. Nilsson, A. A. Konnov, Laminar premixed flat non-stretched lean flames of hydrogen in air, Combust. Flame 162 (10) (2015) 4063–4074.

[3] P. Pelce, P. Clavin, Influence of hydrodynamics and diffusion upon the stability limits of laminar premixed flames, J. Fluid Mech. 124 (1982) 219–237.

[4] A. L. Sanchez, F. A. Williams, Recent advances in understanding of flammability characteristics of hydrogen, Prog. Energ. Combust. 41 (2014) 1–55.

[5] H. F. Coward, F. Brinsley, CLXXIV.–The dilution-limits of inflammability of gaseous mixtures. Part I. The determination of dilution-limits. Part II. The lower limits for hydrogen, methane, and carbon monoxide in air, J. Chem. Soc., Trans. 105 (1914) 1859–1885.

[6] A. L. Furno, E. B. Cook, J. M. Kuchta, D. S. Burgess, Some observations on near-limit flames, Symp. (Int.) Combust. 13 (1) (1971) 593–599.

[7] G. Patnaik, K. Kailasanath, E. S. Oran, Effect of gravity on flame instabilities in premixed gases, AIAA J. 29 (12) (1991) 2141–2148.

[8] C. K. Law, G. M. Faeth, Opportunities and challenges of combustion in microgravity, Prog. Energ. Combust. 20 (1) (1994) 65–113.

[9] I. S. Yakovenko, M. F. Ivanov, A. D. Kiverin, K. S. Melnikova, Large-scale flame structures in ultra-lean hydrogen-air mixtures, Int. J, Hydrogen Energ. 43 (3) (2018) 1894–1901.

[10] Z. Y. Sun, G. X. Li, H. M. Li, Y. Zhai, Z. H. Zhou, Buoyant unstable behavior of initially spherical lean hydrogen-air premixed flames, Energies 7 (8) (2014) 4938–4956.

[11] F. E. Hernández-Pérez, B. Oostenrijk, Y. Shoshin, J. A. van Oijen, L. P. de Goey, Formation, prediction and analysis of stationary and stable ball-like flames at ultra-lean and normal-gravity conditions, Combust. Flame 162 (4) (2015) 932–943.

[12] G. Adomeit, Ignition of gases at hot surfaces under nonsteady-state conditions, Symp. (Int.) Combust. 10 (1) (1965) 237–243.

[13] C. K. Law, H. K. Law, Thermal–ignition analysis in boundary-layer flows, J. Fluid Mech. 92 (1) (1979) 97–108.

[14] C. K. Law, S. H. Chung, Thermal and catalytic inhibition of ignition through reactant depletion, Combust. Sci. Technol. 32 (5–6) (1983) 307–312.

[15] N. M. Laurendeau, Thermal ignition of methane–air mixtures by hot surfaces: A critical examination, Combust. Flame 46 (1982) 29–49.

[16] L. D. Chen, G. M. Faeth, Ignition of a combustible gas near heated vertical surfaces, Combust. Flame 42 (1981) 77–92.

[17] M. M. Yan, L. D. Chen, G. M. Faeth, Analysis of ignition by a plane laminar thermal plume, Combust. Flame 58 (1) (1984) 1–12.

[18] C. Treviño, On the influence of the plate thickness on the boundary layer ignition for large activation energies, Combust. Flame 49 (1–3) (1983) 91–100.

[19] P. L. García-Ybarra, C. Treviño, Analysis of the thermal diffusion effects on the ignition of hydrogen-air mixtures in the boundary layer of a hot flat plate, Combust. Flame 96 (3) (1994) 293–303.

[20] D. Roth, P. Sharma, T. Haeber, R. Schiessl, H. Bockhorn, U. Maas, Ignition by mechanical sparks: ignition of hydrogen/air mixtures by submillimeter–sized hot particles, Combust. Sci. Technol. 186 (10–11) (2014) 1606–1617.

[21] D. Roth, T. Haeber, H. Bockhorn, Experimental and numerical study on the ignition of fuel/air mixtures at laser heated silicon nitride particles, Proc. Combust. Inst. 36 (1) (2017) 1475–1484.

[22] S. Jones, J. Melguizo-Gavilanes, J. E. Shepherd, Ignition by moving hot spheres in H_2-O_2-N_2 environments, Proc. Combust. Inst. 37 (2) (2019) 1597–1604.

[23] J. M. Kuchta, A. Bartkowiak, M. G. Zabetakis, Hot surface ignition temperatures of hydrocarbon fuel vapor–air mixtures, J. Chem. Eng. Data 10 (1965) 282–288.

[24] R. K. Kumar, Ignition of hydrogen–oxygen–diluent mixtures adjacent to a hot, nonreactive surface, Combust. Flame 75 (2) (1989) 197–215.

[25] V. Babrauskas, Ignition handbook, Vol. 318, Fire science publishers, Issaquah, WA, 2003.

[26] M. K. Carmel, Experimental results pertaining to the performance of thermal igniters, Report No. SAND87-3139, available as NUREG/CR-5079, Sandia National Laboratories, 1989.

[27] J. Henrie, A. Postma, Lessons learned from hydrogen generation and burning during the TMI-2 event, Report No. GEND-061, Rockwell Hanford Operations, Rockwell International, 1987.

[28] NAS, Lessons learned from the Fukushima nuclear accident for improving safety of U.S. nuclear plants, National Academies Press, Washington, D.C., 2014.

[29] M. Klauck, E. A. Reinecke, S. Kelm, N. Meynet, A. Bentaïb, H. J. Allelein, Passive auto-catalytic recombiners operation in the presence of hydrogen and carbon monoxide: Experimental study and model development, Nucl. Eng. Des. 266 (2014) 137–147.

[30] A. Bentaïb, N. Meynet, A. Bleyer, Overview on hydrogen risk research and development activities: methodology and open issues, Nucl. Eng. Technol. 47 (1) (2015) 26–32.

[31] C. Treviño, Catalytic ignition of very lean mixtures of hydrogen, Int. J. Hydrogen Energ. 36 (14) (2011) 8610–8618.

[32] N. Meynet, A. Bentaïb, V. Giovangigli, Impact of oxygen starvation on operation and potential gas-phase ignition of passive auto-catalytic recombiners, Combust. Flame 161 (8) (2014) 2192–2202.

[33] A. Fernández, G. M. Arzac, U. F. Vogt, F. Hosoglu, A. Borgschulte, M. C. Jiménez de Haro, O. Montes, A. Züttel, Investigation of a Pt containing washcoat on SiC foam for hydrogen combustion applications, Appl. Catl. B–Environ. 180 (2016) 336–343.

[34] P. A. Boettcher, S. K. Menon, B. L. Ventura, G. Blanquart, J. E. Shepherd, Cyclic flame propagation in premixed combustion, J. Fluid Mech. 735 (2013) 176–202.

[35] P. A. Boettcher, Thermal ignition, Ph.D. thesis, California Institute of Technology (2012).

[36] L. R. Boeck, M. Meijers, A. Kink, R. Mével, J. E. Shepherd, Ignition of fuel-air mixtures from a hot circular cylinder, Combust. Flame 185 (2017) 265–277.

[37] S. A. Coronel, J. Melguizo-Gavilanes, S. Jones, J. E. Shepherd, Temperature field measurements of thermal boundary layer and wake of moving hot spheres using interferometry, Exp. Therm. Fluid Sci. 90 (2018) 76–83.

[38] T. Poinsot, D. Veynante, Theoretical and numerical combustion, Edwards, 2005.

[39] J. Melguizo-Gavilanes, L. R. Boeck, R. Mével, J. E. Shepherd, Hot surface ignition of stoichiometric hydrogen-air mixtures, Int. J. Hydrogen Energ. 42 (11) (2017) 7393–7403.

[40] H. G. Weller, G. Tabor, H. Jasak, C. Fureby, A tensorial approach to computational continuum mechanics using object-oriented techniques, Comput. Phys. 12 (6) (1998) 620–631.

[41] R. Mével, S. Javoy, F. Lafosse, N. Chaumeix, G. Dupré, C. Paillard, Hydrogen-nitrous oxide delay time: shock tube experimental study and kinetic modelling, Proc. Combust. Inst. 32 (1) (2009) 359–366.

[42] R. Mével, S. Javoy, G. Dupré, A chemical kinetic study of the oxidation of silane by nitrous oxide, nitric oxide and oxygen, Proc. Combust. Inst. 33 (1) (2011) 485–492.

[43] R. Mével, J. Melguizo-Gavilanes, L. R. Boeck, J. E. Shepherd, Experimental and numerical study of the ignition of hydrogen-air mixtures by a localized stationary hot surface, Int. J. Heat Fluid Fl. 76 (2019) 154–169.

[44] R. Mével, J. Sabard, J. Lei, N. Chaumeix, Fundamental combustion properties of oxygen enriched hydrogen/air mixtures relevant to safety analysis: Experimental and simulation study, Int. J. Hydrogen Energ. 41 (16) (2016) 6905–6916.

[45] C. M. Vagelopoulos, F. N. Egolfopoulos, C. K. Law, Further considerations on the determination of laminar flame speeds with the counterflow twin-flame technique, Symp. (Int.) Combust. 25 (1) (1994) 1341–1347.

[46] K. T. Aung, M. I. Hassan, G. M. Faeth, Flame stretch interactions of laminar premixed hydrogen/air flames at normal temperature and pressure, Combust. Flame 109 (1-2) (1997) 1–24.

[47] R. W. Pitz, S. Hu, P. Wang, Tubular premixed and diffusion flames: effect of stretch and curvature, Prog. Energ. Combust. 42 (2014) 1–34.

[48] F. A. Williams, J. F. Grcar, A hypothetical burning-velocity formula for very lean hydrogen–air mixtures, Proc. Combust. Inst. 32 (1) (2009) 1351–1357.

[49] S. M. Candel, T. J. Poinsot, Flame stretch and the balance equation for the flame area, Combust. Sci. Technol. 70 (1-3) (1990) 1–15.

[50] M. Matalon, On flame stretch, Combust. Sci. Technol. 31 (3-4) (1983) 169–181.

[51] P. Wang, J. A. Wehrmeyer, R. W. Pitz, Stretch rate of tubular premixed flames, Combust. Flame 145 (1-2) (2006) 401–414.

[52] B. Savard, Characterization and modeling of premixed turbulent n-heptane flames in the thin reaction zone regime, Ph.D. thesis, California Institute of Technology (2015).

Supplemental material

Figure 14 shows ignition in 8% hydrogen-air mixture, leading to a cyclic (puffing) flame. This phenomenon was investigated in detail by Boettcher et al. [34].

Figure 15 shows ignition in 12% hydrogen-air mixture, leading to an expanding flame.

Figure 16 shows single-puff ignition in 5% hydrogen-air mixture. The ignition source in this experiment was a 0.4 mm Kanthal A-1 wire supported by a ceramic tube. The wire ignited the mixture at a surface temperature of 1112 K after a heating time of 493 ms. Single-puff ignition and plume formation are similar to the observations from the glow plug. Time scales and leading-edge flame shape differ due to differences in thermal plume extent and strength.

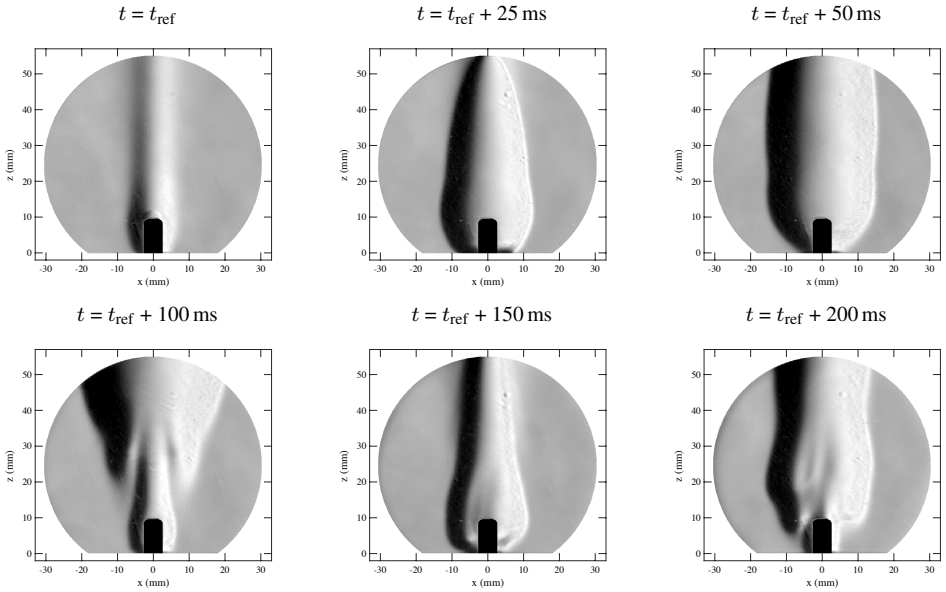

Figure 14: High-speed schlieren sequence of ignition in 8% hydrogen-air mixture; Puffing flame.

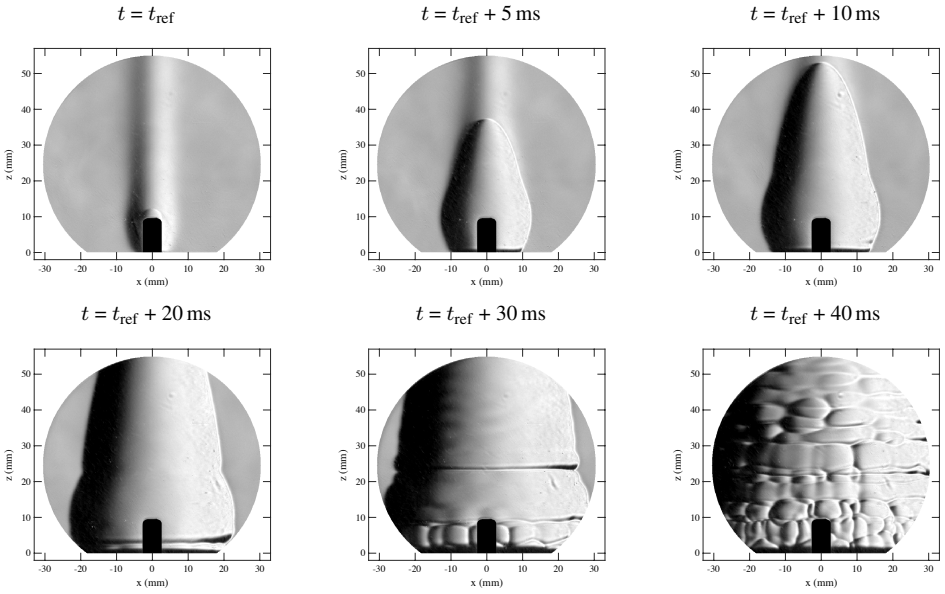

Figure 15: High-speed schlieren sequence of ignition in 12% hydrogen-air mixture; Expanding flame.

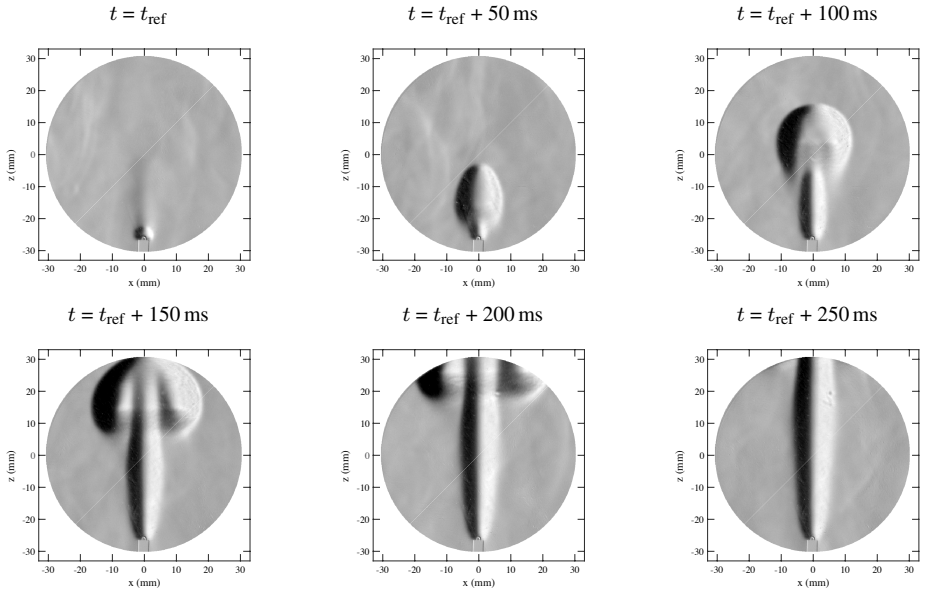

Figure 16: High-speed schlieren sequence of ignition from a u-shaped hot wire (diameter 0.2 mm; exposed length 3 mm) supported from below by a ceramic tube in 5% hydrogen-air mixture; Singe-puff ignition.